

A comparison of the Voyager 1 ultraviolet spectrometer and plasma science measurements of the Io plasma torus

M. H. Taylor,¹ N. M. Schneider,¹ F. Bagenal,¹ B. R. Sandel,²
D. E. Shemansky,³ P. L. Matheson,³ and D. T. Hall⁴

Abstract. We have developed a sophisticated package (Colorado Io Torus Emissions Package, or CITEP) to simulate emissions from the Io plasma torus, and have used it to examine the consistency of Voyager in situ and remote observations. CITEP merges ion composition derived from the ultraviolet spectrometer line ratios with measurements of electron densities, electron temperatures, and ion temperatures obtained by the plasma science instrument. The program then predicts the brightness and morphology of torus EUV emissions. We find that the measured brightness is approximately 2 times larger than the model predicts. When scaled up by this factor, the morphology of the model radial emission profile is consistent with the data, but somewhat less sharply peaked at the ribbon location. We examine several possible causes for the brightness discrepancy such as calibration errors, measurement accuracy, inaccuracies of the model, and torus variability, but find no definitive cause.

1. Introduction

An empirical model of the composition and temperature of the Io plasma torus surrounding Jupiter was created by using Voyager 1 in situ and remote observations [Bagenal, 1994]. Our objective is to use the Voyager model to simulate the plasma torus emissions, and compare the synthetic emissions with remote observations to gain a better understanding of conditions in the torus. In this paper we take the first step in this process by comparing the simulated emissions from the Voyager model with the actual remote observations from Voyager.

The Io plasma torus is composed primarily of electrons and sulfur and oxygen ions which originate from Io and corotate with Jupiter's magnetic field (see reviews by Belcher [1983] and Brown *et al.* [1983]). Kupo *et al.* [1976] first detected the torus from ground-based observations of S⁺ visible lines. In 1979, Voyager 1 provided measurements of the composition and energy of the torus plasma with its plasma science (PLS) in-

strument [Bridge *et al.*, 1979] and remotely measured EUV emissions with its ultraviolet spectrometer (UVS) [Broadfoot *et al.*, 1979]. These measurements revealed the torus' complex spatial and temporal structure, including two distinct radially separated regions: a hot, outer region and a cold, inner region [Bagenal and Sullivan, 1981]. The cold region inward of ~ 5.6 Jovian radii (R_J) consists mostly of S⁺ and O⁺ ions with temperature $T_i \lesssim 15$ eV and electrons with $T_e \lesssim 4$ eV. The hot region outside $5.6 R_J$ consists mostly of O⁺, S⁺, and S²⁺ ions with $T_i \sim 60$ eV and electrons with $T_e \gtrsim 5$ eV. A narrow band of emissions in the hot torus between 5.6 and $6.0 R_J$ is called the "ribbon" region [Trauger, 1984]. The remote Voyager observations show that the torus brightness and position vary with time, longitude, and local time [Sandel and Broadfoot, 1982; Dessler and Sandel, 1992]. Other spacecraft and ground-based observations have confirmed the complexity of the torus system [Schneider and Trauger, 1994; Strobel, 1989], leading to the need for a comprehensive torus model which can be compared with the ongoing observations.

The Voyager model was created by combining the Voyager 1 UVS and PLS data sets. Combining the remote and in situ data is difficult owing to the line-of-sight averaging through the complex torus structure inherent in the remote observations, but necessary owing to the limitations of each of the data sets. The PLS measurements provide electron densities, electron temperatures, and ion temperatures along the spacecraft trajectory from 12 to $5 R_J$, but are unable to provide ion composition between 12 and $5.6 R_J$. A UVS radial scan of the torus was used to determine ion partitioning in this region by using line ratios but not individual line brightnesses [Bagenal *et al.*, 1992]. Shemansky

¹Laboratory for Atmospheric and Space Physics, University of Colorado, Boulder.

²Lunar and Planetary Laboratory, University of Arizona, Tucson.

³Space Sciences Institute, University of Southern California, Los Angeles.

⁴Center for Astrophysical Sciences, The Johns Hopkins University, Baltimore, Maryland.

[1987] has extensively analyzed a subset of the UVS data we examine here to determine ion partitioning in the ribbon region (see also *Shemansky and Smith* [1981]). The longitudinally and temporally invariant model is designed to be a starting point for developing more complex models and a reference for examining the observed temporal variability. We used the Voyager empirical model combined with computer-simulated emissions to attempt to simulate the UVS observations. Our specific goals were to simulate the UVS brightnesses and morphology near the ribbon, neither of which was used in creating the empirical torus model. The computer simulation facilitates the comparison of torus models with remote observations by calculating the line-of-sight integrations using accurate observing geometry.

We present our analysis in the following manner. In section 2 we discuss the Voyager UVS observations. In section 3 we discuss the computer simulation used to model the observations. In section 4 we discuss the results and their implications, and in section 5 we give the summary and conclusions.

2. Observations

The Voyager 1 UVS instrument is an objective grating spectrograph which takes a 126-channel spectrum in the wavelength range 540–1700 Å. A complete description of the instrument is given by *Broadfoot et al.* [1977]. In the few weeks surrounding the Jupiter encounter, hundreds of thousands of spectra were taken of the torus. Count rates were low ($\lesssim 100$ counts per second per spectrum), so spectra are averaged together to increase the signal-to-noise ratio. A scattering matrix operator is applied to the spectra to compensate for internal scattering of photons by the instrument. Figure 1 shows a typical torus spectrum consisting of an average of ~ 50 spectra taken during 200 s of observation 4 days prior to closest approach. All of the significant emissions observed by the UVS originate from the hot torus where the electron temperature favors EUV emissions. This particular spectrum was taken while pointing at the ribbon region.

In our analysis we examine the torus emissions of five major EUV features labeled in Figure 1. The feature at 1256 Å was not modeled, since the contribution of hydrogen Lyman α sky background emissions at 1216 Å is uncertain. We sum the counts for each channel range shown in Figure 1 to further reduce the noise. The channel ranges were not chosen to include all of the signal under each feature, since each feature consists of the sum of several lines, but rather to minimize the number of contributing lines while still maintaining a reasonable signal-to-noise ratio. We examine 880 spectra taken near the dusk ansa (point of maximum elongation at 1630 Jovian local time) between 1845 and 1943 spacecraft event time on day 60 of 1979 (SCET 1979–60/1845 to 60/1943). *Shemansky* [1987] and *Shemansky and Smith* [1981] analyze a subset of this data consisting of the average of all spectra taken between 1900 and 1930 SCET. During this time period the dusk

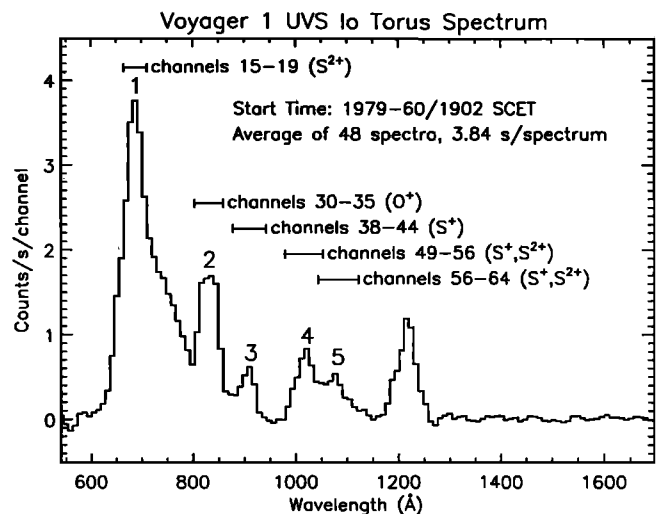


Figure 1. Voyager 1 UVS spectrum of the Io torus. The spectrum is an average of 48 spectra taken while the UVS slit was pointed at $5.83 \pm 0.075 R_J$ projected distance from Jupiter. The total integration time was 184 s, and the system III longitude of the observed portion of the torus was $\sim 310^\circ$. The background and scattered photons have been removed from the spectrum. The five features and their channel ranges used in our analysis are labeled. The wavelength limits from the low-wavelength edge of the first channel to the high edge of the last are as follows: channels 15–19, 664.5–710.8 Å; channels 30–35, 803.4–858.9 Å; channels 38–44, 877.5–942.3 Å; channels 49–56, 979.3–1053.4 Å; channels 56–64, 1044.2–1118.2 Å. Note that the channel ranges do not necessarily include all of the signal under each feature (see text).

ansa was at Jupiter System III longitude $\sim 310^\circ$, and the spacecraft was at a range of $67.5 R_J$ from Jupiter. The UVS slit is $0.86^\circ \times 0.10^\circ$, giving a projected slit size of $1.0 \times 0.12 R_J$. The long axis of the slit was tilted 20° clockwise from the Jovian rotation axis as shown in Figure 2. The slit scanned radially inward from 6.5 to $4.1 R_J$ in projected distance from Jupiter. The vertical position of the slit varied from $0.3 R_J$ below the Jovian rotational equator to $0.7 R_J$ above. This range of pointing and the slit field of view are shown superimposed with a contour plot of simulated torus emissions in Figure 2.

We determine absolute pointing from the scan platform positions recorded in the UVS spectral headers by applying a correction computed by using an imaging science system wide-angle image taken at SCET 1979–60/1819, 26 min prior to the start of the UVS scans. The image included the same part of the Jupiter system as the UVS scans, and scan platform motion between it and the UVS scans was minimal. We used the image to determine the true position of Io relative to the UVS field. To compute the correction, we compared this with the relative position inferred for the same time from the pointing information in the UVS header and the position of Io determined by using the Jet Propulsion Laboratory (JPL) spacecraft position instrument constants

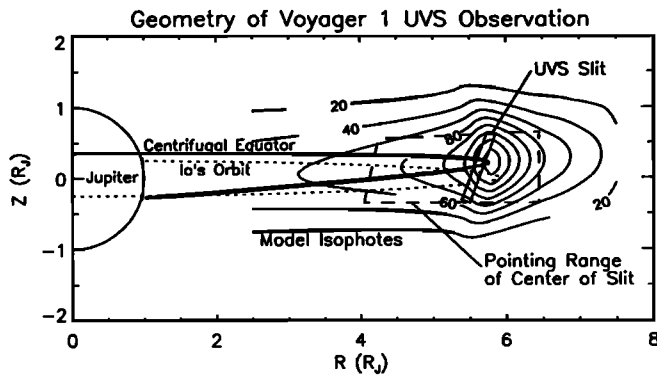


Figure 2. Geometry of the Voyager 1 UVS system scan of the torus at SCET 1979–60/~1900. The figure indicates the position of Io's orbit and the centrifugal equator at the time of observation. The contour lines indicate model isophotes showing the position and brightness in rayleighs of the torus seen by channels 15–19 (feature 1) of the UVS at the time of observation. The solid rectangle indicates the size and orientation of the UVS field of view during the observation. The dashed trapezoid indicates the range of pointing of the center of the UVS field of view during the system scan.

events (SPICE) system. The correction was $0.15 R_J$ measured in the plane of Io's orbit, and $0.35 R_J$ perpendicular to the plane. This procedure yields absolute pointing that is correct to better than $0.05 R_J$, about one third of the bin size. Relative pointing during the scans is known to better than $0.02 R_J$.

Radial emission profiles created from the torus scan are shown in Figures 3a–3e. The spectra taken during the scan were averaged in $0.15 R_J$ bins of projected distance from the Jovian rotational axis. Approximately 50 spectra were averaged for each bin. The figures show that the torus brightness reaches a maximum near the ribbon region at $\sim 5.7 R_J$. The error bars shown in the figures are determined by using Poisson statistics applied to the number of photoevents recorded over the channel range during the total integration time of the ~ 50 spectra.

3. Modeling

We have created a computer program to facilitate the comparison of Io torus plasma models with remote observations of torus emissions. The Colorado Io Torus Emissions Package (CITEP) originated from the MAGPAC software package created at JPL to aid in planning for the Galileo mission [Balcom *et al.*, 1991]. Improvements were made on the MAGPAC software by including a more complex magnetic field model, more accurate atomic physics, and the updated Voyager torus model (created by using more accurate plasma physics and a more complete analysis of plasma conditions). CITEP simulates emissions from the torus at a specified wavelength as seen from a specified position, enabling a direct comparison of the Voyager empirical model with remote observations.

First, CITEP creates a three-dimensional model of plasma densities and temperatures by using an input file of densities and temperatures on the centrifugal equator (the point along a magnetic field line which is farthest from the Jovian rotation axis). For this analysis the Voyager torus model is used, but the program permits other torus models. The relevant Voyager plasma parameters on the centrifugal equator are shown in Figure 4. The plasma distribution along magnetic field lines is calculated by numerically solving diffusive equilibrium equations which balance centrifugal, pressure, magnetic, and electric forces, in the same manner as that of *Bagenal* [1994] (hereafter B94). The resulting plasma model is identical to B94 except for the following minor differences. A second, hot electron population given by B94 is included in the plasma distribution but not in the calculation of emission rate coefficients. The hot electrons' effect on torus emissions will be discussed in section 4. Also, B94 uses the "O4 plus current sheet" Jovian magnetic field model [Connerney *et al.*, 1982] to obtain the plasma distribution, while CITEP uses the "O4" model without a current sheet. This difference does not alter the plasma distribution significantly inward of $8 R_J$ (B94). Following B94, we assume for this analysis that the torus is longitudinally symmetric.

The volume emission rate at each location in the torus is determined from the calculated plasma distribution and emission rate coefficients. A program, COREQ (for COLLisional and Radiative EQUilibrium), calculates the emission rate coefficients, $C_i(T_e, n_e)$, for the major ion species in the torus by balancing electron-ion collisional excitation with radiative and collisional de-excitation in an optically thin plasma. Rate equations describing transitions between fine-structure states are solved simultaneously. The index i denotes the emission multiplet, and n_e is the electron density. The method described by *Shemansky and Smith* [1981] is used with updated atomic data, assuming a single thermal distribution of electrons (see also *Shemansky* [1987] and *Shemansky* [1980a]). Emission probabilities for the ions S^+ , S^{2+} , S^{3+} , O^+ , and O^{2+} are calculated by using the local electron density n_e . The local ion density, n_i , is then multiplied by these probabilities to obtain a volume emission rate at each location in the torus. Emission rate coefficients for each of the major multiplets from this analysis at three temperatures are given in Table 1.

CITEP integrates the term $C_i n_e n_i dl$ along the line of sight of the observer through the torus to compute the model brightnesses. The line-of-sight integration step size dl is typically $0.05 R_J$. The observer's position, pointing, and the wavelength of the emission are all specified by the user. By specifying a two-dimensional array of pointing directions, the user can create a computer-simulated image of the torus. The CITEP image can then be compared with actual images of the torus, or convolved with a slit sensitivity function to estimate the brightness seen at the specified wavelength by a spectrometer on an encounter spacecraft such as Voyager or Galileo, an Earth-orbit spacecraft

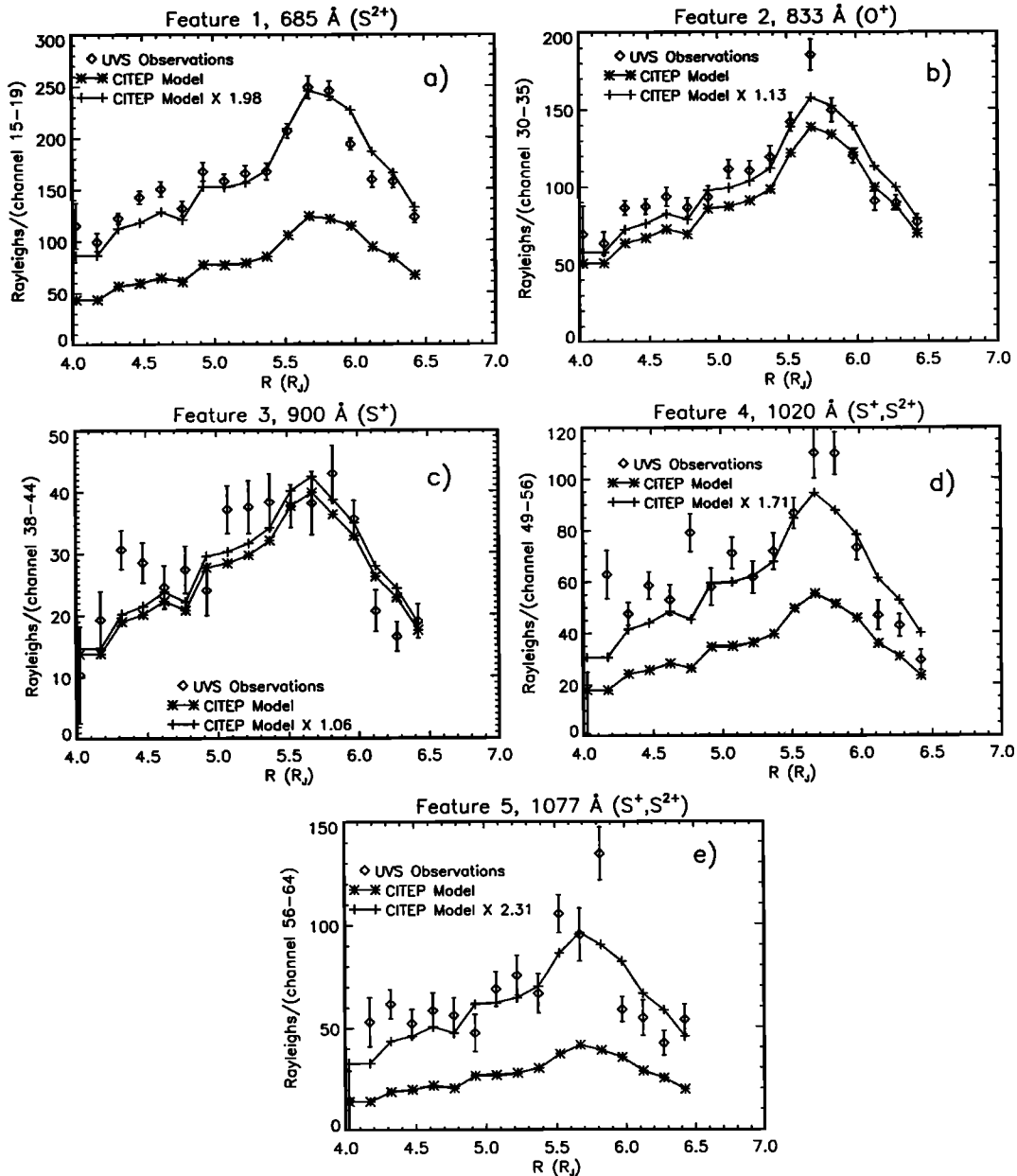


Figure 3. (a) Observed and modeled radial profile of Io torus emissions near 685 Å, UVS channels 15–19 (feature 1). The modeled emissions are shown both in absolute brightness and scaled to match the weighted mean brightness of the observations. The errors bars on the data points are one-sigma error bars from photon noise based on the total number of photoevents measured. (b) Observed and modeled emissions near 833 Å, UVS channels 30–35 (feature 2). (c) Observed and modeled emissions near 900 Å, UVS channels 38–44 (feature 3). (d) Observed and modeled emissions near 1020 Å, UVS channels 49–56 (feature 4). (e) Observed and modeled emissions near 1077 Å, UVS channels 56–64 (feature 5).

such as the International Ultraviolet Explorer (IUE) or Hubble Space Telescope (HST), or ground-based optical observations. The strong spatial variability of the torus, as shown in Figure 2, shows that this full-image convolution is required.

CITEP was meticulously checked against simple calculations and models used by other investigators. The calculated line intensities were checked independently at many points covering the range of parameters in the

torus by using various torus models with square cross sections and constant densities and temperatures. For example, CITEP predicts that a $5-R_J$ path through a S^{2+} plasma with $n_e = 1000 \text{ cm}^{-3}$, $n_{S^{2+}} = 300 \text{ cm}^{-3}$, and $T_e = 5 \text{ eV}$ (58,000 K) emits 17.3 R in the 13 to 1 transition (678–682 Å) of Table 1, consistent with calculations by hand. In addition an explicit check of CITEP's line-of-sight brightness integral was performed with two independently constructed torus mod-

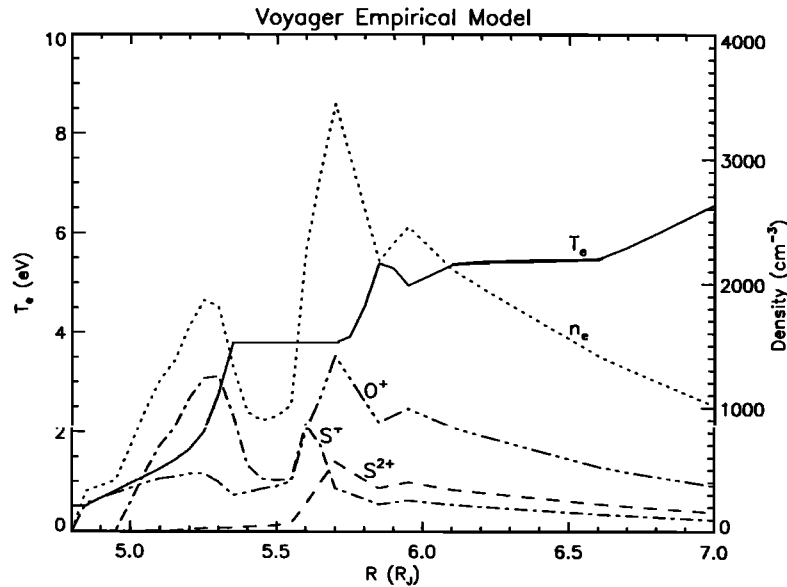


Figure 4. Radial profile of ion densities, electron density, and electron temperature from the Voyager empirical torus model (see text; *Bagenal* [1994]).

els [*Thomas, 1992; Matheson and Shemansky, 1994*], and they agree within 3%.

We modeled the radial profiles discussed in section 2 by combining CITEP images with the UVS pointing information. COREQ spectra were convolved with a UVS slit function (reasonably approximated by a triangle with full width at half maximum (FWHM) of 32 Å) to determine the contribution, or weight, of each line of the major transitions to the appropriate UVS channel range. Although certain transitions lie outside the channel ranges, they still contribute signal if the line centers lie within a FWHM of a channel range. All multiplets contributing $\geq 0.1\%$ of the total signal in each channel range are given in Table 2 along with their relative weight. Feature 1 consists mostly of S^{2+} emissions. Feature 2 consists mostly of O^+ emissions, and feature 3 consists mostly of S^+ emissions. Features 4 and 5 have approximately equal parts of S^+ and S^{2+} emissions. The convolved spectra are used by CITEP to create images of the torus emissions in each of the channel ranges. We created five CITEP images, one for each feature, for each 10-min interval of the ~ 1 -hour observing time, using the appropriate viewing geometry for each interval. This time resolution sufficiently removes observational effects caused by the motion of the torus as it rotates. A CITEP image of feature 1, channels 15–19, used in the analysis is shown in Figure 5. For each of the 880 UVS observations, we modeled the observed brightness by averaging across a $1.0 \times 0.12 R_J$ UVS slit overlaid with the appropriate CITEP image at the appropriate position. We then averaged the modeled brightnesses in $0.15 R_J$ radial bins, mimicking the analysis of the data. The resulting model radial profiles are shown in Figures 3a–3e.

In addition to the UVS data, we modeled two IUE torus observations to aid in our discussion of the UVS

calibration. SWP-4448 was an 8.7-hour observation starting 1979, day 60, 1931 UT. SWP-4463 was a 7.4-hour observation starting day 62, 1326 UT. The $10'' \times 20''$ slit ($0.46 \times 0.92 R_J$) was fixed on the Jovian rotational equator at a distance of $4.5 R_J$ west of Jupiter for SWP-4448 and $5.9 R_J$ west of Jupiter for SWP-4463. No attempt was made to track the torus ansa with the slit, so as the torus rotated, it wobbled in and out of the slit. CITEP is essential for removing the geometrical effects of such an observation. Two wavelength features of the IUE spectra were modeled: S^+ emission at 1256 Å and S^{2+} emission at 1729 Å. The IUE brightnesses were obtained from an updated reduction by D. T. Hall of the torus observations discussed by *Moos et al.* [1985]. For SWP-4448 the brightnesses were $B(1256\text{Å}) = 51 \pm 8 R$ and $B(1729\text{Å}) = 68 \pm 10 R$. For SWP-4463 the brightnesses were $B(1256\text{Å}) = 64 \pm 10 R$ and $B(1729\text{Å}) = 58 \pm 9 R$. The errors given are typical 15% temporal variations in the brightness. Figure 6 shows the results of the CITEP modeling of these observations.

4. Results and Discussion

We find that the measured brightness is approximately a factor of 2 brighter than the model. Increasing the model brightness of each spectral feature to match the mean data brightness, we obtain a reasonable fit to the radial emission profile, although the data tends to have a narrower peak. We have also calculated the total radiative power output from the torus, using CITEP and the Voyager empirical torus model, and we obtain a value of 1.6×10^{12} W compared to frequently quoted values of $2\text{--}3 \times 10^{12}$ W [e.g. *Strobel, 1989*]. We separate our discussion into two parts, the first discussing

Table 1. Emission Rate Coefficients

Ion	Index ^a	Transition ^b	λ , Å ^c	C_i^d		
				34,800 K	58,000 K	81,200 K
S ⁺	1,4	$3p^3\ ^4S^0-3p^4\ ^4P$	1251–1260	1.02(-9)	2.71(-9)	3.86(-9)
	1,7	$-4s\ ^4P$	907–913	1.47(-10)	8.26(-10)	1.76(-9)
	1,8	$-3d\ ^4F$	903–908	2.29(-10)	9.30(-10)	1.52(-9)
	2,6	$3p^3\ ^2D^0-3d\ ^2P$	1097–1102	1.71(-10)	6.75(-10)	1.11(-9)
	2,9	$-4s\ ^2P$	1014–1020	1.13(-10)	5.19(-10)	9.28(-10)
	2,11	$-3d\ ^2F$	996–1001	8.70(-11)	3.72(-10)	6.29(-10)
	2,13	$-4s\ ^2D$	937–938	2.65(-11)	1.28(-10)	2.28(-10)
	2,15	$-3d\ ^2G$	891	4.17(-11)	1.78(-10)	2.78(-10)
	2,22	$-3d\ ^2D$	841–844	2.40(-11)	1.38(-10)	2.64(-10)
	2,24	$-3d\ ^2F$	809	6.77(-11)	4.21(-10)	8.33(-10)
	2,39	$-4d\ ^2F$	705–708	5.06(-12)	4.20(-11)	9.43(-11)
	2,44	$-3p^4\ ^2P$	692–695	3.55(-11)	3.26(-10)	7.64(-10)
	3,9	$3p^3\ ^2P^0-4s\ ^2P$	1124–1132	2.96(-11)	1.36(-10)	2.43(-10)
	3,22	$-3d\ ^2D$	915–919	1.05(-11)	6.02(-11)	1.15(-10)
S ²⁺	1,4	$3p^2\ ^3P-3p^3\ ^5S$	1713,1729	1.17(-9)	2.21(-9)	2.63(-9)
	1,6	$-3p^3\ ^3P^0$	1013–1021	2.45(-10)	1.04(-9)	1.84(-9)
	1,9	$-3p^3\ ^3S^0$	724–729	1.99(-10)	1.57(-9)	3.64(-9)
	1,11	$-3d\ ^3P^0$	699–703	1.78(-10)	1.63(-9)	4.13(-9)
	1,12	$-4s\ ^3P^0$	681–685	7.18(-11)	7.15(-10)	1.89(-9)
	1,13	$-3d\ ^3D^0$	678–682	1.62(-10)	1.61(-9)	4.25(-9)
	2,7	$3p^2\ ^1D-3d\ ^1D^0$	1077	1.45(-10)	5.73(-10)	9.32(-10)
	2,8	$-3p^3\ ^1P^0$	797	9.81(-12)	6.71(-11)	1.39(-10)
S ³⁺	1,3	$3p\ ^2P^0-3p^2\ ^2D$	1063–1074	6.99(-10)	2.57(-9)	4.24(-9)
	1,4	$-3p^2\ ^2S$	810,816	1.32(-10)	9.74(-10)	2.27(-9)
	1,6	$-3d\ ^2D$	657–661	1.73(-10)	1.75(-9)	4.54(-9)
O ⁺	1,4	$2p^3\ ^4S^0-2p^4\ ^4P$	833–834	2.63(-10)	1.61(-9)	3.43(-9)
	2,5	$2p^3\ ^2D^0-2p^4\ ^2D$	718–719	1.10(-11)	1.15(-10)	2.86(-10)
	3,5	$2p^3\ ^2P^0-2p^4\ ^2D$	797	1.27(-12)	1.32(-11)	3.29(-11)
O ²⁺	1,5	$2p^2\ ^3P-2p^3\ ^3D^0$	833–835	2.59(-10)	1.49(-9)	2.99(-9)
	1,6	$-2p^3\ ^3P^0$	702–704	7.89(-11)	6.68(-10)	1.60(-9)

^aTransition index used by COREQ to mark energy levels from lowest to highest; 1 indicates the ground state.

^bLower energy level appears first.

^cVacuum wavelength range of the line centers of each transition (multiplet).

^dEmission rate coefficients (in cubic centimeters per second) for electron density $n_e = 1000\text{ cm}^{-3}$ and indicated electron temperature. These coefficients were calculated by using COREQ, an electron impact excitation model (see text). Here, 1(-12) = 1×10^{-12} .

the morphology of the fit and the second discussing the absolute brightness discrepancy.

4.1. Morphology

We obtain information from the model fit to the data despite the difference in absolute brightness. First, for those features with the highest signal-to-noise ratio (features 1, 2, and 4), the modeled position of the peak matches the observed position within $0.1 R_J$, although the modeled peak is somewhat wider than observed. This suggests that the peak in plasma densities in the Voyager model at $5.7 R_J$ (Figure 4) is in the correct position, since emissions in the torus are directly proportional to $n_e n_i$, as discussed in section 3. The match in peak position is perhaps fortuitous, since Voyager 2

UVS observed $\pm 0.2 R_J$ radial variations in the peak position versus longitude [Dessler and Sandel, 1992; hereafter DS92]. A more detailed discussion of the peak position requires an examination of many Voyager 1 UVS scans of the torus.

Second, the peak in the data profile is about 20% narrower than the model at 75% of the maximum brightness for the three profiles with the highest signal-to-noise ratio (Figures 3a, 3b, and 3d). This might suggest a need for a narrower peak in the $n_e(r)n_i(r)$ profile. We found, using CITEP, that narrowing the density profile by 30% produced a 20% narrowing in the emission profile; however, altering the T_e profile or including longitudinal variations could also change the width, so a unique solution is not possible.

The observed longitudinal variation in peak position of DS92 would affect the ribbon width determined from in situ measurements because the measurements were made over a range of longitudes. As Voyager approached Jupiter and passed through the ribbon, its System III longitude was increasing. DS92 show that the ribbon was significantly farther from Jupiter at the longitude where Voyager entered the ribbon than where it left. PLS would therefore report a broader ribbon than actually exists. Voyager approached Jupiter at a rate $0.023 R_J/\text{degree}$ in System III longitude. Since, at the Voyager longitude, the Jupiter-ribbon distance decreases at the rate of $0.0019 R_J/\text{degree}$, PLS would report a ribbon about 10% too broad. This effect is in the same sense as the difference in peak widths we found, though of somewhat smaller magnitude.

4.2. Brightness

Figure 6 gives the brightness discrepancy versus wavelength showing that the UVS and IUE data are typically a factor of 2 brighter than the model. The brightness discrepancy is significant for five of the seven wavelengths modeled. The discrepancy is also apparent in Table 2, where we compare our results directly with the UVS brightnesses published by *Shemansky* [1987]. We discuss possible explanations for the discrepancy, including UVS instrumental effects, differing plasma conditions, and variabilities.

4.2.1. Calibration. The accuracy of the UVS absolute intensity calibration has been under dispute for some time and may contribute to the brightness discrepancy, but is probably not the sole cause. *Holberg et*

Table 2. Transition Brightnesses and Weighting

Ion	λ , Å	Weight ^a	Brightness, R			
			CITEP ^b (Weighted)	CITEP ^c (Total)	S87 ^d (In-Flight)	S87 ^e (Preflight)
<i>Feature 1,^f Channels 15–19, 664.5–710.8 Å</i>						
S ⁺	705–708	0.614	0.56	0.91		
	692–695	0.848	5.11	6.03		
S ²⁺	724–729	0.139	4.97	35.77	40	53
	699–703	0.737	28.16	38.21	101	130
	681–685	0.867	14.72	16.97 ^g	86	106
	678–682	0.815	31.11	38.17 ^g		
S ³⁺	657–661	0.337	2.07	6.16	47	56
O ⁺	718–719	0.306	2.94	9.62		
O ²⁺	702–704	0.689	1.54	2.24		
<i>Feature 2,^f Channels 30–35, 803.4–858.9 Å</i>						
S ⁺	841–844	0.871	2.65	3.04		
	809	0.639	5.88	9.21		
S ²⁺	797	0.329	0.49	1.49		
S ³⁺	810,816	0.752	2.48	3.29		
O ⁺	797	0.329	0.36	1.11		
	833–834	0.944	86.83	91.98 ^g	120	200
O ²⁺	833–835	0.944	4.02	4.25 ^g		
<i>Feature 3,^f Channels 38–44, 877.5–942.3 Å</i>						
S ⁺	907–913	0.980	12.53	12.78 ^g	34 ^h	57 ^h
	903–908	0.975	12.48	12.79 ^g		
	915–919	0.962	1.27	1.32 ^g		
	937–938	0.621	1.95	3.13		
	891	0.812	2.67	3.29		
<i>Feature 4,^f Channels 49–56, 979.3–1053.4 Å</i>						
S ⁺	1014–1020	0.995	8.58	8.63 ^g	65	108
	996–1001	0.884	7.46	8.43 ^g		
S ²⁺	1013–1021	0.993	22.70	22.86 ^g		
	1077	0.052	0.64	12.31		
S ³⁺	1063–1074	0.191	1.47	7.67		

Table 2. (continued)

Ion	λ , Å	Weight ^a	Brightness, R			
			CITEP ^b (Weighted)	CITEP ^c (Total)	S87 ^d (In-Flight)	S87 ^e (Preflight)
<i>Feature 5,^f Channels 56–64, 1044.2–1118.2 Å</i>						
S ⁺	1014–1020	0.025	0.22	8.63		
	1124–1132	0.517	1.17	2.26		
	1097–1102	0.968	9.75	10.07 ^g		
S ²⁺	1013–1021	0.034	0.78	22.86		
	1077	0.993	12.22	12.31 ^g		
S ³⁺	1063–1074	0.932	7.15	7.67 ^g	68	102

^aFraction of the signal from each transition which contributes to the corresponding UVS channel range.

^bModel CITEP brightness in rayleighs weighted by the previous column and averaged over a subset of the radial profile to match the analysis of *Shemansky* [1987].

^cTotal model CITEP brightness in rayleighs of each transition, obtained by dividing the previous column by the weighting in column 3.

^d*Shemansky* [1987] UVS brightnesses adjusted by the in-flight calibration. This column can be compared directly to the previous column to obtain approximately the brightness discrepancies plotted in Figure 6.

^e*Shemansky* [1987] UVS brightnesses from his Table A1, using the preflight calibration, obtained from a subset of the data analyzed here (see text).

^fFeature number refers to labels in Figure 1. Wavelength range is from the low-wavelength edge of the first UVS channel to the high edge of the last channel.

^gAll of these transitions contribute to the listed S87 brightness for each feature. A proper comparison can be made with S87(in-flight) by summing these *g*-superscripted transitions. All of the signal for feature 5 was attributed to the S³⁺ multiplet by *Shemansky* [1987], but we find brighter contributions from S⁺ and S²⁺.

^hThe brightness of this feature as published by *Shemansky* [1987] and *Shemansky and Smith* [1981] was found to be in error and is here corrected.

al. [1991] have revised the sensitivity upward 40–60% from the preflight calibration in the wavelength range 912–1150 Å based on in-flight comparisons with rocket measurements of hot subluminescent stars. Holberg scales

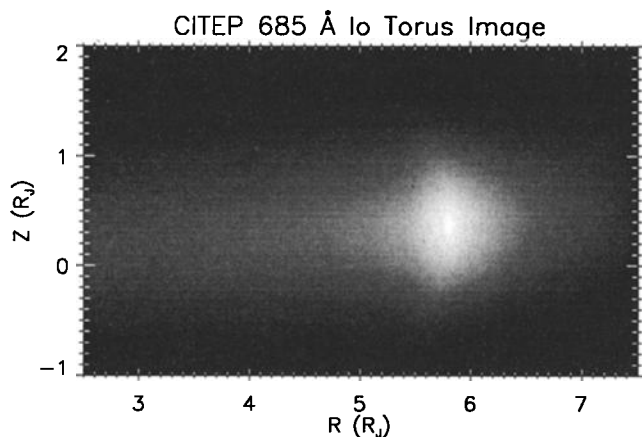


Figure 5. CITEP simulated 685-Å image as would be seen from the Voyager 1 spacecraft at SCET 1979–60/1900, in UVS channels 15–19. The peak intensity from the ansa point is 170 R. UVS would have observed twice the brightness, or 340 R.

the correction from 60% at 912 Å down to 0% at 550 Å based on a rocket measurement of the white dwarf HZ 43 at 520 Å [*Holberg et al.*, 1982]. We use the Holberg in-flight calibration in our analysis of the UVS spectra. The preflight calibration would give a brightness difference of a factor of 2.5 (Table 2). The discrepancy persists even longward of 912 Å, where the UVS has been cross-calibrated with other instruments. We also find the same factor of 2 difference in our modeling of data from IUE (Figure 6), which has been calibrated extensively, suggesting the problem is not simply calibration errors.

4.2.2. Atomic data. A second possible explanation for the brightness difference is inaccurate collision strengths. The original sources for the atomic data quote uncertainties that are electron energy dependent, but generally less than 20% at the transition energies of interest here. Nevertheless, faulty collision strengths should randomly alter the brightnesses rather than favor consistently lower brightnesses at all lines of all ion species. This suggests these inaccuracies are not the cause for the difference.

4.2.3. Density. A third possible explanation is inaccurate plasma density. The plasma density must be

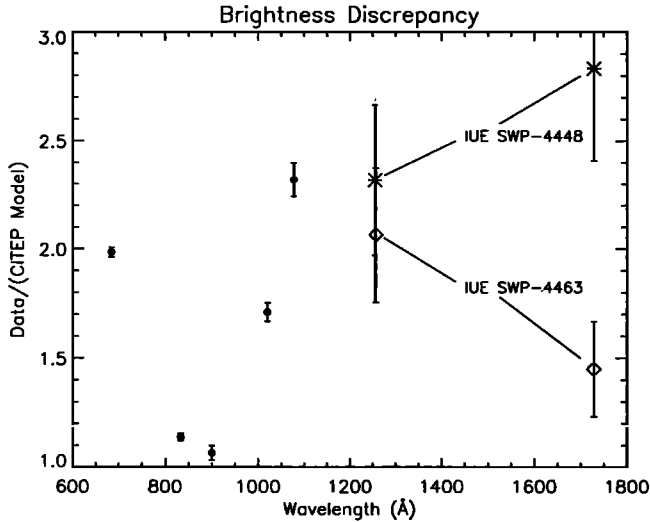


Figure 6. Brightness discrepancy (data/CITEP model) versus wavelength. Error bars for the UVS points are one-sigma error bars of the weighted mean brightness of the data. Uncertainties in the UVS measurements include only counting statistics. IUE error bars are typical 15% temporal variations in the brightness.

increased by more than 30% to approximate the feature brightnesses. The Voyager planetary radio astronomy instrument made simultaneous measurements of electron density in the Io torus which agree with the PLS measurements to an accuracy of about 10% [Warwick *et al.*, 1979; Birmingham *et al.*, 1981]. Furthermore, no shift of composition can match the intensities of all the features. It is therefore unlikely that inaccurate plasma density is the sole cause of the brightness discrepancy.

4.2.4. Thermal electron temperature. A fourth possible explanation is inaccurate thermal electron temperature T_e . Inside $5.75 R_J$, measurements of T_e were not possible owing to instrument limitations. Sittler and Strobel [1987] estimate 15% uncertainty in their determination of T_e outside $5.75 R_J$, where the brightness discrepancy is also evident. We require a 35% increase in T_e between 5.7 and $6.5 R_J$ to increase the 685-Å brightness sufficiently. If T_e uncertainty estimates are correct, then inaccurate T_e is not the culprit.

4.2.5. Hot electrons. A fifth possible explanation is the contribution of the hot electron population to emissions, which is not present in the CITEP calculations. The total charge fraction of hot (100 eV) electrons in the ribbon region is estimated to be $0.15 \pm 0.075\%$ from the PLS data (B94). Including 0.3% hot electrons in the calculations gives only a 6% increase in brightness, implying that a 5% hot electron fraction would be required to double the emissions. The amount of 100-eV electrons is constrained by the composition of the torus as well as the error estimate of the PLS measurements. A 5% hot electron fraction would produce an unreasonably large S^{2+}/S^+ ratio for most ion chemistry models [Shemansky, 1980b, 1987]. It may be possible that a significant population of nonthermal electrons with temperatures lower than 100 eV are consistent with the PLS measurements. A 10% fraction of 20-eV electrons would be sufficient to boost the 685-Å

emissions by a factor of 2, but such a population would thermally equilibrate with the main thermal component rapidly (approximately a few minutes). Therefore a continuous 20-eV electron source would be required to maintain the population, making its existence unlikely. Very recently, Meyer-Vernet *et al.* [1995] reported variations of T_e with latitude in the Ulysses in situ measurements between 7 and $8 R_J$ which obey an approximate polytrope law $T_e \propto 1/\sqrt{n_e}$. We have estimated that if such a strong latitudinal gradient in T_e holds all the way in to the ribbon, the total brightness would be greater than that actually measured. Further study of possible latitudinal T_e gradients is in progress.

4.2.6. Longitudinal variation. A sixth possible explanation is longitudinal variation in brightness. As noted in section 4.1, the PLS data and UVS observations were taken $\sim 100^\circ$ apart in longitude. The UVS brightnesses of our analysis are consistent with the average dusk ansa brightness during the Voyager 1 encounter, implying that PLS took in situ data at a longitude greatly diminished in density or electron temperature from the average. Short-lived System III longitudinal variations in 685-Å brightness [Sandel and Broadfoot, 1982] and variations with a slightly longer period than System III (termed System IV) [Sandel and Dessler, 1988] are typically less than 30%, insufficient to account for the brightness difference. In addition, a large longitudinal variation interpreted as radial structure in the Voyager model would result in a poor fit to the radial profile between 5.7 and $6.5 R_J$ as discussed in section 4.1.

4.2.7. Temporal variation. A seventh possible explanation is temporal variation in brightness. Rapid brightness variation on timescales of less than one rotation (10 hours) were observed by Voyager 1 UVS during days 89–96 of 1979 and by Voyager 2 UVS during days 115–160 of 1979. During these time periods the torus brightnesses were still comparable to those observed by Voyager 1 on day 60, when the data used in this analysis were taken [Sandel *et al.*, 1979]. For the hundreds of Voyager 1 and 2 observations examined, the standard deviation in brightness was only 15% with the brightness never deviating more than 40% from the mean. Using CITEP to model an observation from the Voyager 2 data set at 685 Å, we found the CITEP brightness was 4.28 standard deviations below the mean value, making it 99.993% unlikely.

5. Conclusions

Five of the seven major EUV wavelength features we investigated are approximately a factor of 2 brighter than were predicted by our CITEP model. The scaled-up radial profile computed from the model fits the measured profile reasonably well, although the data have a somewhat narrower peak, suggesting that radial variations are more prominent than in the Voyager model. The absolute brightness difference cannot be accounted for by any single plausible inaccuracy in the Voyager model or the CITEP model, or by the kinds of longitudinal and temporal variations commonly seen in the

torus. It is possible, though unlikely, that a combination of changes in plasma parameters within acceptable limits, for example, increasing the electron temperature 15% and the plasma density 10%, may achieve a nearly sufficient increase in brightness. Calibration errors and inaccuracies in atomic data also seem unable to account for the brightness discrepancy, but further work should be done to better quantify their accuracy. Also, further work is needed to determine the consistency of a ~20-eV hot electron component with the PLS data. Comparison of the Voyager model with other observations in the UV and visible will help to determine possible causes for the discrepancy.

Acknowledgments. The authors are grateful to M. Harel and D. Balcom for their help in obtaining and understanding the JPL MAGPAC software. Also, we wish to thank A. J. Dessler, J. B. Holberg, M. A. McGrath, R. L. McNutt, and N. Thomas for valued discussions and help in verification of our computer code. We also thank C. W. Hord and the Galileo EUV/UVS team, without whose support this research would not have been possible. This research was supported by NASA under JPL/Galileo contract 958675 and Planetary Atmospheres grant NAGW-2484. B.R.S. acknowledges support under NASA contract NAGW-3657. CITEP software and documentation are currently available for distribution by contacting M.H.T. via the Internet at taylor@torus.colorado.edu.

The Editor thanks two referees for their assistance in evaluating this paper.

References

- Bagenal, F., Empirical model of the Io plasma torus, 1, Voyager measurements, *J. Geophys. Res.*, **99**, 11,043, 1994.
- Bagenal, F., and J. D. Sullivan, Direct plasma measurements in the Io torus and inner magnetosphere of Jupiter, *J. Geophys. Res.*, **86**, 8447, 1981.
- Bagenal, F., D. E. Shemansky, R. L. McNutt Jr., R. Schreier, and A. Eviatar, The abundance of O⁺⁺ in the Jovian magnetosphere, *Geophys. Res. Lett.*, **19**, 79, 1992.
- Balcom, D., M. Harel, M. Ruderman, and L. Fischer, Magpac User's Guide, *JPL Publ. 625-646*, Jet Propul. Lab., Pasadena, Calif., 1991.
- Belcher, J. W., The low-energy plasma in the Jovian magnetosphere, in *Physics of the Jovian Magnetosphere*, edited by A. J. Dessler, pp. 68-105, Cambridge Univ. Press, New York, 1983.
- Birmingham, T. J., J. K. Alexander, M. D. Desch, R. F. Hubbard, and B. M. Pedersen, Observations of electron gyroharmonic waves and the structure of the Io torus, *J. Geophys. Res.*, **86**, 8497, 1981.
- Bridge, H. S., et al., Plasma observations near Jupiter: Initial results from Voyager 1 encounter with Jupiter, *Science*, **204**, 972, 1979.
- Broadfoot, A. L., et al., Ultraviolet spectrometer experiment for the Voyager mission, *Space Sci. Rev.*, **21**, 183, 1977.
- Broadfoot, A. L., et al., Extreme ultraviolet observations from Voyager 1 encounter with Jupiter, *Science*, **204**, 979, 1979.
- Brown, R. A., C. B. Pilcher, and D. F. Strobel, Spectrophotometric studies of the Io torus, in *Physics of the Jovian Magnetosphere*, edited by A. J. Dessler, pp. 197-225, Cambridge Univ. Press, New York, 1983.
- Connerney, J. E. P., M. H. Acuña, and N. F. Ness, Voyager 1 assessment of Jupiter's planetary magnetic field, *J. Geophys. Res.*, **87**, 3623, 1982.
- Dessler, A. J., and B. R. Sandel, System III variations in apparent distance of Io plasma torus from Jupiter, *Geophys. Res. Lett.*, **19**, 2099, 1992.
- Holberg, J. B., W. T. Forrester, D. E. Shemansky, and D. C. Barry, Voyager absolute far-ultraviolet spectrophotometry of hot stars, *Astrophys. J.*, **257**, 656, 1982.
- Holberg, J. B., B. Ali, T. E. Carone, and R. S. Polidan, Absolute far-ultraviolet spectrophotometry of hot subliminous stars from Voyager, *Astrophys. J.*, **375**, 716, 1991.
- Kupo, I., Y. Mekler, and A. Eviatar, Detection of ionized sulfur in the Jovian magnetosphere, *Astrophys. J. Lett.*, **205**, L51, 1976.
- Matheson, P. L., and D. E. Shemansky, Chemistry and transport in the Io torus ramp, Submitted to *Icarus*, 1994.
- Meyer-Vernet, N., M. Moncuquet, and S. Hoang, Temperature inversion in the Io plasma torus, *Icarus*, in press, 1995.
- Moos, H. W., T. E. Skinner, S. T. Durrance, P. D. Feldman, M. C. Festou, and J.-L. Bertaux, Long-term stability of the Io high-temperature plasma torus, *Astrophys. J.*, **294**, 369, 1985.
- Sandel, B. R., and A. L. Broadfoot, Io's hot plasma torus—A synoptic view from Voyager, *J. Geophys. Res.*, **87**, 212, 1982.
- Sandel, B. R., and A. J. Dessler, Dual periodicity of the Jovian magnetosphere, *J. Geophys. Res.*, **93**, 5487, 1988.
- Sandel, B. R., et al., Extreme ultraviolet observations from Voyager 2 encounter with Jupiter, *Science*, **206**, 962, 1979.
- Schneider, N. M., and J. T. Trauger, The structure of the Io torus, *Astrophys. J.*, in press, 1995.
- Shemansky, D. E., Radiative cooling efficiencies and predicted spectra of species of the Io plasma torus, *Astrophys. J.*, **236**, 1043, 1980a.
- Shemansky, D. E., Mass-loading and diffusion-loss rates of the Io plasma torus, *Astrophys. J.*, **242**, 1266, 1980b.
- Shemansky, D. E., Ratio of oxygen to sulfur in the Io plasma torus, *J. Geophys. Res.*, **92**, 6141, 1987.
- Shemansky, D. E., and G. R. Smith, The Voyager 1 EUV spectrum of the Io plasma torus, *J. Geophys. Res.*, **86**, 9179, 1981.
- Sittler, E. C., Jr., and D. F. Strobel, Io plasma torus electrons: Voyager 1, *J. Geophys. Res.*, **92**, 5741, 1987.
- Strobel, D. F., Energetics, luminosity, and spectroscopy of Io's torus, in *Time Variable Phenomena in the Jovian System*, *NASA Spec. Publ., SP-494*, pp. 183-195, 1989.
- Thomas, N., Optical observations of Io's neutral clouds and plasma torus, *Surv. Geophys.*, **13**, 91, 1992.
- Trauger, J. T., The Jovian nebula: A post-Voyager perspective, *Science*, **226**, 337, 1984.
- Warwick, J. W., et al., Voyager 1 planetary radio astronomy observations near Jupiter, *Science*, **204**, 995, 1979.

F. Bagenal, N. M. Schneider, and M. H. Taylor, Laboratory for Atmospheric and Space Physics, University of Colorado, Campus Box 392, Boulder, CO 80309-0392. (e-mail: bagenal@dosxx.colorado.edu; schneider@pele.colorado.edu; taylor@torus.colorado.edu)

D. T. Hall, Center for Astrophysical Sciences, Dept. of Physics and Astronomy, The Johns Hopkins University, Baltimore, MD 21218. (e-mail: dthall@pha.jhu.edu)

P. L. Matheson and D. E. Shemansky, Space Sciences Institute, University of Southern California, Los Angeles, CA 90089-1191. (e-mail: matheson@athena.usc.edu; dons@athena.usc.edu)

B. R. Sandel, Lunar and Planetary Laboratory, University of Arizona, Tucson, AZ 85721. (e-mail: sandel@vega.lpl.arizona.edu)

(Received May 9, 1994; revised March 29, 1995; accepted April 3, 1995.)